ACS APPLIED MATERIALS & INTERFACES

Research Article

www.acsami.org

Cellulose Nanoparticles as Modifiers for Rheology and Fluid Loss in Bentonite Water-based Fluids

Mei-Chun Li,[†] Qinglin Wu,*[,†] Kunlin Song,[†] Yan Qing,[‡] and Yiqiang Wu*[,‡]

[†]School of Renewable Natural Resources, Louisiana State University AgCenter, Baton Rouge, Louisiana 70803, United States

[‡]College of Materials Science and Engineering, Central South University of Forestry and Technology, Changsha 410004, China

ABSTRACT: Rheological and filtration characteristics of drilling fluids are considered as two critical aspects to ensure the success of a drilling operation. This research demonstrates the effectiveness of cellulose nanoparticles (CNPs), including microfibrillated cellulose (MFC) and cellulose nanocrystals (CNCs) in enhancing the rheological and filtration performances of bentonite (BT) water-based drilling fluids (WDFs). CNCs were isolated from MFC through sulfuric acid hydrolysis. In comparison with MFC, the resultant CNCs had much smaller dimensions, more negative surface charge, higher stability in aqueous solutions, lower viscosity, and less evident shear thinning behavior. These differences resulted in the distinctive microstructures between MFC/BT- and CNC/BT-WDFs. A typical "core−shell" structure was created in CNC/BT-WDFs due to the strong surface interactions among BT layers, CNCs, and immobilized water molecules. However, a similar structure was not formed in MFC/BT-WDFs. As a result, CNC/BT-WDFs had superior rheological properties, higher temperature stability, less fluid loss volume, and thinner filter cakes than BT and MFC/BT-WDFs. Moreover, the presence of polyanionic cellulose (PAC) further improved the rheological and filtration performances of CNC/BT-WDFs, suggesting a synergistic effect between PAC and CNCs.

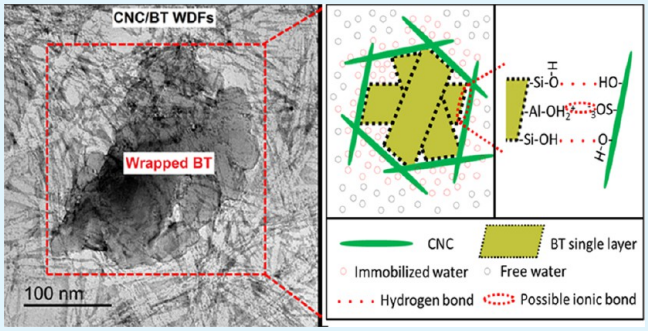

KEYWORDS: *microfibrillated cellulose, cellulose nanocrystals, bentonite, water-based drilling fluids, rheology, filtration loss*

INTRODUCTION

Drilling fluids perform critical roles in oil and gas drilling operations, such as carrying cuttings from the bottom of wellbore to the surface, suspending cuttings from sedimentation, cooling drilling pipes and bits, reducing friction between formation and drilling equipment, stabilizing wellbore, and avoiding formation collapse.[1−5] Besides these functions, ideal drilling fluids should also be cheap, low reactive, noncorrosive, health safe, and environmentally friendly, and have excellent tolerance to the salt and temperature.[6−9] Depending on the composition, drilling fluids are mainly classified into three types, i.e., water-based drilling fluids (WDFs), oil-based drilling fluids (ODFs), and synthetic drilling fluids (SDFs). Although ODFs and SDFs have better capacity to maintain the stability of wellbore and to lubricate the drilling pipe and bit, the development of WDFs is the future considering environmental and economic effect.[10,11] Furthermore, the advantages of WDFs also include good cooling and cutting removal ability, and fast formation breaking-down rate.

WDFs are usually composed of water, clay, rheology modifier, and fluid loss controller. Among many types of clays, bentonite (BT) is commonly used in WDFs due to its outstanding swelling capacity and superior rheological properties.[12] In WDFs, the presence of BT improves the viscosity via edge-to-face attraction, and forms a compact filter cake, which helps prevent the fluid invasion into the formation. In general, a large amount of BT is required to obtain the desired rheological and filtration properties. Meanwhile, the incorporation of too much BT also creates much thicker filter cakes, which could cause serious formation damage and pipe sticking problems, and hence reduce the drilling productivity.[13,14] To overcome these drawbacks, polymer-based rheological modifier and fluid loss reducer are normally applied. In recent years, various types of natural or synthetic polymers, such as starch,[15] guar gum,[16] xanthan gum,[17] carboxymethyl cellulose (CMC),[18] polyanionic cellulose (PAC),[19] amphoteric cellulose,[20] rice husk,[9] polyacrylamide,[8] and polyacrylates,[21] have been used as a rheological modifier and fluid loss reducer in WDFs.

Currently, nanotechnology is recognized as "the next industrial revolution", which has a far-reaching effect on almost every industry and even all aspects of our daily life. The extra-large surface area to volume ratio results in superior or even unexpected performances for surface-dependent nanomaterials. The utilization of various nanoparticles, such as graphene,[5] carbon nanotube,[22] silica,[23] and metal oxides,[12,14] as a rheological modifier and fluid loss reducer in WDFs, has been studied for several years. Superior rheological properties were obtained by using very low concentration of nanoparticles

Received: January 16, 2015
Accepted: February 13, 2015
Published: February 13, 2015

DOI: 10.1021/acsami.5b00498
ACS Appl. Mater. Interfaces 2015, 7, 5006−5016

(usually <1.0 wt %). More importantly, it has been reported that nanoparticles had a higher possibility of plugging pore throats in shale than microparticles,[23] leading to a significant reduction in the fluid invasion as well as thinner filter cakes, which are advantageous for the maintenance of formation stability and drilling productivity. Nevertheless, most of the previously reported nanoparticles are inorganic materials, which are insoluble, nonbiodegradable, and somewhat detrimental to the health of drilling operators. Inorganic nanoparticles can pass through tissues of living organisms and never be metabolized. Therefore, in order to minimize the environmental hazard and health risk as well as to reduce the cost, it is very essential to develop clean, cheap, renewable, recyclable, biodegradable, and environmentally friendly nanoparticles as additives in WDFs.

As one of the most abundant and promising materials on the earth, cellulose has received great interest. Cellulose nanoparticles (CNPs), primarily including microfibrillated cellulose (MFC), and cellulose nanocrystals (CNCs), can be isolated from many cellulosic resources, such as wood, plants, marine animals, algae, and bacteria using different preparation methods. MFC can be produced by enzyme hydrolysis, mechanical disintegration, and 2,2,6,6-tetramethyl-1-piperidinyloxy (TEMPO) mediated oxidation methods.[24−26] MFC has dimensions of 10−20 nm in width and several micrometers in length, yielding very large aspect ratios and highly entangled networks. CNCs can be fabricated using a strong acid hydrolysis method, which show a rod- or needle-like shape 10−20 nm in width and 50−500 nm in length.[27−29] Because of their nanoscale dimensions, CNPs have a large specific surface area up to several hundred m^2/g, leading to a considerable amount of interaction and superior fluid properties at a relatively low concentration. Moreover, due to the large aspect ratio and the self-assembling ability to form multilayer membranes, CNPs have been used as gas barrier agent to improve the gas permeability of papers, films and composites.[30−32] These intrinsically appealing features enable CNPs to act as an effective additive in WDFs.

The specific objective of this research was to develop novel, green, cheap, renewable, safe, and environmentally friendly CNPs as rheological modifier and fluid loss reducer for BT-WDF application, and understand the contributions of CNPs' properties, including morphology, surface charge and dispersion state to the final performances of BT-WDFs. Two types of CNPs, including MFC and CNCs with different concentrations ranging from 0.1 to 1.0 wt %, were applied as additives to improve the rheological and filtration properties of BT-WDFs. The influence of MFC and CNCs on the fluid properties was directly contrasted. Considerable differences between two materials were demonstrated and correlated with their dispersion microstructures. In order to demonstrate the effectiveness of CNCs, the performances of CNC/BT-WDFs were compared with those of BT-WDFs with higher BT concentrations. Additionally, the synergistic effect of PAC and CNCs on the performance improvement in the BT-WDFs was also studied.

EXPERIMENTAL SECTION

Materials. Wyoming sodium BT (AQUAGEL GOLD SEAL, dry-powdered, 200 mesh) was supplied from Baroid Industrial Drilling Products Inc. (Houston, TX). CNCs were hydrolyzed from MFC (Celish KY 100-S grade, 25% solid content, Daicel Chemical Industries, Ltd., Tokyo, Japan) using 64 wt % sulfuric acid for 4 h, followed by high-pressure homogenization treatment according to our previous report.[33] Low viscosity PAC (PAC-L, Hallibuton Company, Houston, TX) was used as filtration control agent. Hydrochloric acid and sodium hydroxide (Fisher Scientific Company, Pittsburgh, PA) were used as pH value adjuster. Sulfuric acid was supplied from Sigma-Aldrich Corp. (St. Louis, MO).

Preparation of BT, MFC/BT, CNC/BT and PAC/CNC/BT Fluids. Never-dried MFC and CNC samples were dispersed in aqueous solution with vigorous mechanical stirring at a speed of 2000 rpm for 1 h. The resultant suspensions were diluted into 0.1, 0.25, 0.5, and 1.0 wt % using deionized water. Then, 3 wt % of BT powders based on the weight of the CNP suspensions were slowly added into the suspensions, followed by vigorously mechanical stirring at a speed of 10000 rpm for 1 h. For the purpose of comparison, two series of WDFs, i.e., BT (3, 6, 7.5, 9, 12, and 15 wt %) and PAC/CNC/BT (0.5/0.5/3 and 0.1/0.5/3 wt %), were also prepared.

Characterization of CNPs. The morphology of CNPs was taken using transmission electron microscopy (TEM, JEM 1400, JEOL) at an accelerating voltage of 120 kV. The average dimension of CNPs was calculated, based on 50 randomly selected CNPs from the TEM micrographs using ImageJ 1.47 software (http://rsb.info.nih.gov.libezp.lib.lsu.edu/ij/). For the sample preparation, CNP suspensions were diluted to 0.1 wt % using deionized water, followed by ultrasonic treatment for 1 h. Then, a droplet (5 μL) of 0.1 wt % CNP suspensions was deposited onto a 300-mesh Lacey carbon film grid (LC300-CU-100). A drop of 2 wt % uranyl acetate solution was placed on the CNP coated grid to stain the CNPs for about 2 min. The zeta potential values of CNP suspensions were measured using a ZetaTrac analyzer (MicroTrac Inc., Largo, FL). Before each run, the concentration of CNP suspensions was adjusted to 0.05 wt %. For each sample, ten measurements were carried out, and the average value was calculated. X-ray photoelectron spectroscopy (XPS) was recorded for each freeze-dried CNP sample using a Specs PHOIBOS-100 spectrometer (SPECS, Berlin, Germany) with an Al Kα irradiation (1486.61 eV) at 10 kV and 10 mA. Survey scans were conducted from 1200 to 0 eV with pass energy of 40 eV and scan step of 1.0 eV. Using the SpecLab software, the mass concentration of C, O, and S elements was obtained. The molecular formula of sulfuric acid-treated CNCs can be expressed as $C_6H_{10}O_5$-$(SO_3)_n$.[34] Therefore, the number (n) of sulfate groups in 100 bulk anhydroglucose units was determined using the following equation:

$$n = \frac{100 \times 162.14 \times S}{32.065 - 80.065 \times S} \quad (1)$$

where S (wt %) is the mass concentration of sulfur atom detected from the XPS.

Microstructures of MFC/BT- and CNC/BT-WDFs. The microstructures of MFC/BT- and CNC/BT-WDFs were also taken using TEM (JEM 1400, JEOL) at an accelerating voltage of 120 kV. The sample preparation procedure was the same as this used for CNPs described previously.

Rheological Properties of WDFs. Two types of viscometers were used to measure the rheological properties of WDFs. A stress-controlled rheometer (AR 2000, TA Instrument Inc., New Castle, DE) equipped with DIN concentric cylinders geometries was applied to measure the rheological properties of MFC/BT- and CNC/BT-WDFs. The DIN concentric cylinders geometry consists of a stainless steel cup and a rotator. The diameters of stainless steel cup and rotator are 30.38 and 28.02 mm, respectively. Before each measurement, suspensions were vigorously stirred for 20 min and then approximate 20 mL samples were carefully placed into the stainless steel cup. The steady-flow shear viscosity was measured in the shear range of 0.1 to 1200 s^{-1} at 25 °C. The influence of pH on the viscosity was studied with pH values of 4.4, 6.7, 8.9, and 11 in the shear range of 0.1 to 1200 s^{-1} at 25 °C. The pH values of WDFs were carefully adjusted using 1 M HCl and 0.5 M NaOH solutions. The influence of temperature on the viscosity was investigated in the temperature range of 25 to 80 °C with a fixed shear rate of 10 s^{-1}.

For non-Newtonian fluids, many mathematical models have been applied to fit the relationship between shear stress and shear rate.

DOI: 10.1021/acsami.5b00498
ACS Appl. Mater. Interfaces 2015, 7, 5006−5016

Table 1. Physicochemical Characteristics of CNPs

samples	width (nm)	length (nm)	aspect ratio	ζ-potential (mV)	sulfur content (wt %)	OSO_3H/100 anhydroglucose units
MFC	12.5 ± 8.4	>1000	>80	−4.6 ± 1.2	0	0
CNCs	6.1 ± 3.5	228.4 ± 63.8	37.8 ± 15.2	−35.4 ± 2.0	0.53	2.72

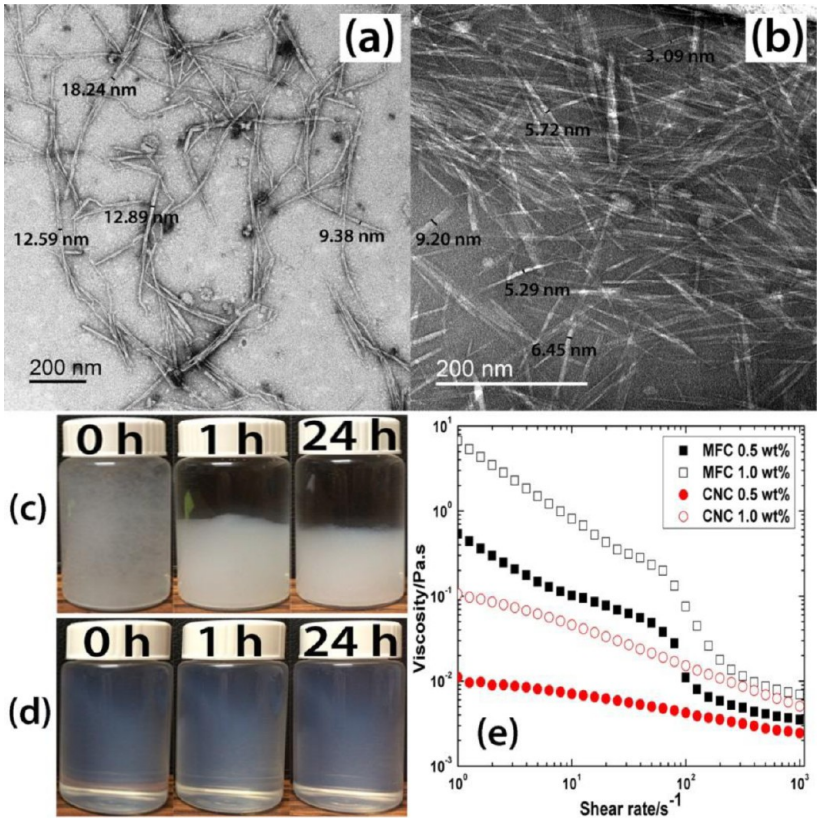

Figure 1. Characterization of CNPs: (a and b) TEM micrographs of MFC and CNCs, respectively; (c and d) dispersion states of MFC and CNCs in aqueous solution at the concentration of 1.0 wt % after 0, 1, and 24 h, respectively; (e) shear-thinning behaviors of MFC and CNC suspensions at the concentrations of 0.5 and 1.0 wt %.

Among these models, Bingham, power-law and Herschel−Bulkey models are commonly used.[35] The Bingham plastic model is given by eq 2.

$$\tau = \tau_0 + \mu_p \times \dot{\gamma} \quad (2)$$

where τ is the shear stress, τ_0 is the yield stress or yield point, μ_p is the plastic viscosity, and $\dot{\gamma}$ is the shear rate. With the Bingham plastic model, the yield point and plastic viscosity can be easily obtained. However, for a complex drilling fluid, the Bingham plastic model was found to be inadequate, because the relationship between the shear stress and shear rate is no longer linear. To overcome this drawback, a power-law model is developed, as expressed by eq 3.

$$\tau = K \times \dot{\gamma}^n \quad (3)$$

where K is the flow consistency coefficient, and n is the flow behavior index. With the power-law model, the flow consistency coefficient and flow behavior index can be easily obtained. However, it was found that due to the lack of yield point, the power-law model was not accurate to fit the rheological curves, especially at the low shear rates. Therefore, the Herschel−Bulkey model, which is a combination of Bingham plastic and power-law models, was developed, as given by eq 4.

$$\tau = \tau_0 + K \times \dot{\gamma}^n \quad (4)$$

To characterize the fluid properties based on industrial practice, a rotating viscometer (NL Baroid, NL Industries, Inc., Houston, TX) was used to measure the viscosity (i.e., apparent viscosity-AP, and plastic viscosity-PV), yield point (YP), as well as timed gel strength (i.e., initial gel strength-Gel_{in}, and 10 min gel strength-Gel_{10min}) of the BT, CNC/BT and PAC/CNC/BT-WDFs. The viscosity measurements were conducted at fixed rates of 600 and 300 rpm, and then AP, PV, and YP were calculated according to the following equations:

$$AP = \theta_{600}/2 \quad (5)$$

$$PV = \theta_{600} - \theta_{300} \quad (6)$$

$$YP = \theta_{300} - PV \quad (7)$$

where $\theta_{600}$and θ_{300} are the dial readings at 600 and 300 rpm, respectively. The Gel_{in} and Gel_{10min} were recorded as the maximum dial reading at a fixed rate of 3 rpm after standing undisturbed for 10 s and 10 min, respectively.

Filtration Properties of WDFs. Filtration tests were carried out in a standard filter press equipment (Model No. 30201, Fann Instrument Co., Houston, TX) with Fann filter papers (Part No. 206051, Fann Instrument Co., Houston, TX) according to the API guidelines.[36] This type of filter paper has the particle size retention range from 2 to 5 μm. In each run, 100 mL of the WDFs was placed in the filter press at room temperature under a pressure of 100 psi (0.69 MPa) provided by N_2O gas chargers (Whip-it Brand, South San Francisco, CA). The volumes of filtrate through the filter paper were determined at 1.0, 7.5, 15, 20, and 30 min after starting each measurement.[5] When the measurement finished, the filter paper was carefully removed from the filter press and a photograph was taken immediately. The filter paper was then set out at room temperature for 24 h to evaporate the water from the filter cake. Finally, the thickness of each filter cake was

DOI: 10.1021/acsami.5b00498
ACS Appl. Mater. Interfaces 2015, 7, 5006−5016

measured using an electronic caliper (Pro-Max, Fowler High Precision, Newton, MA) and recorded in millimeters (mm). The surface morphology of each filter cake was performed using field emission scanning electron microscopy (FE-SEM, a FEI QuantaTM 3D FEG dual beam SEM/FIB system, Hillsboro, OR) at a 20 kV accelerating voltage. Before observation, each sample was gold-coated using a sputter coater.

RESULTS AND DISCUSSION

The physicochemical properties of CNPs are summarized in Table 1, and their TEM micrographs are displayed in Figure 1. Native MFC exhibited highly entangled network, consisting of individual microfibrils and microfibril bundles (Figure 1a). The individual microfibrils were 12.5 ± 8.4 nm in width and a few micrometers in length, resulting in an extremely high aspect ratio value (>80). CNCs showed a needle-like morphology with an average width of 6.1 ± 3.5 nm and length of 228.4 ± 63.8 nm (Figure 1b). Its aspect ratio was estimated to be 37.8 ± 15.2. During the sulfuric acid hydrolysis process, negatively charged sulfate groups ($-O-SO_3^-$) were introduced on the surface of CNCs, which were confirmed by the ζ-potential and XPS analysis.[37] MFC and CNC suspensions had ζ-potential values of −4.6 ± 1.2 and −35.4 ± 2.0 mV, respectively. The introduction of sulfate groups on the surface of CNCs led to a considerable change in the zeta potential. Generally, a stable colloid has a threshold value of ≥+30 or ≤−30 mV, whereas a colloid with low ζ-potential ranging from 0 to ±5 mV tends to flocculate quickly.[38] Therefore, the microfibrils quickly precipitated within 1 h in aqueous solution (Figure 1c), while the CNC suspensions exhibited high stability for 24 h (Figure 1d). The mass content of S element on CNC surface from XPS anaylysis was determined as 0.53 wt %, equivalent to 2.72 sulfate groups per 100 anhydroglucose units. Figure 1e shows the steady-state viscosity versus shear rate for MFC and CNC suspensions at concentrations of 0.5 and 1.0 wt %. Both MFC and CNC suspensions exhibited low viscosity at high shear rates, but high viscosity at low shear rates; which are commonly known as "shear-thinning" fluids.[39] The shear-thinning phenomenon became more significant as the concentration of CNPs increased from 0.5 to 1.0 wt %. In comparison to CNC suspensions, MFC suspensions displayed more marked shear-thinning behavior and much higher viscosity at the same concentration. It can be therefore concluded that the characteristics, including morphology, surface properties, and rheological behaviors between MFC and CNCs significantly varied, which might lead to distinctive performances in the CNP-based materials.

Drilling fluids are commonly shear-thinning non-Newtonian fluids, which have high viscosity at low shear rates to carry or suspend the cuttings from the wellbores, but low viscosity at high shear rates to be rapidly pumped into the bottom of wellbores as well as to easily release the cuttings. Rheological analysis (Figure 1e) indicated that both MFC and CNC suspensions have good shear-thinning properties, which are well-suitable for well drilling fluid application. Therefore, this phenomenon inspired us to apply CNPs as novel rheological modifiers in BT-WDFs. The concentration of CNPs in BT-WDFs was varied in the range of 0.1 to 1.0 wt % to monitor how effective the CNPs would modify the rheological properties of BT-WDFs. The concentration of BT was fixed as 3.0 wt %. As a result, the maximum solid content is only 4 wt %, which is generally classified as the low-solid drilling fluids.[40] The benefits of using low-solid drilling fluids include high rate of penetration, low friction on the surface of pump equipment, thin filter cake, and great shale stability. However, the low-solid drilling fluids were quite sensitive to the ions, such as Ca^{2+}, Na^+, Cl^-, and CO_3^{2-}, which naturally exist in the formation.

Figure 2a,b shows the plots of viscosity versus shear rate for MFC/BT- and CNC/BT-WDFs at different CNP concentrations, respectively. Without the addition of CNPs, BT-WDFs exhibited almost a Newtonian rheological behavior in a wide range of shear rates from 0 to 200 s^{-1}, i.e., the viscosity remained constantly as the increase in the shear rate. Surprisingly, in the high shear rates (>200 s^{-1}), a shear thickening behavior appeared. The shear thickening behavior was also observed in starch/water mixture, polystyrene–ethylacrylate colloidal latex, and silica/poly(ethylene oxide) solution.[41−43] Hoffman[44] proposed that the shear thickening behavior was attributed to the microstructure arrangement from order to disorder induced by the applied shear force. Khandavalli[43] postulated that the shear thickening behavior in silica/poly(ethylene oxide) solution was ascribed to the formation of hydroclusters as a result of polymer–particle interaction induced by the applied shear force, too. Anyway, in the drilling fluid application, the shear thickening behavior should be avoided in order to achieve good pumpability and easily release the cuttings at high shear rates. Gratifyingly, when the CNPs were incorporated, the shear-thickening behavior was prohibited and gradually disappeared as the concentrations of CNPs increased from 0.1 to 1.0 wt %. More importantly, the addition of CNPs effectively increased the viscosity of BT-WDFs and led to more pronounced shear-thinning behavior, which was advantageous for the drilling fluid application. For example, at a shear rate of 10 s^{-1}, the addition of 1.0 wt % MFC

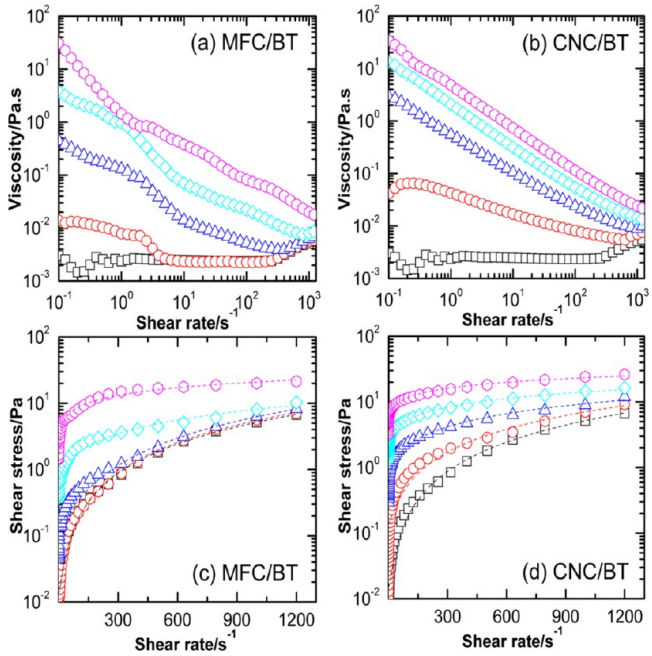

Figure 2. Plots of viscosity versus shear rate for (a) MFC/BT-, and (b) CNC/BT-WDFs. Shear stress versus shear rate for (c) MFC/BT-, and (d) CNC/BT-WDFs at different CNP concentrations: 0 wt % (black squares), 0.1 wt % (red circles), 0.25 wt % (blue triangles), 0.5 wt % (cyan diamonds) and 1.0 wt % (magenta hexagons). (Dash lines in panels c and d represent the fitted lines using Herschel–Bulkley model).

DOI: 10.1021/acsami.5b00498
ACS Appl. Mater. Interfaces 2015, 7, 5006−5016

Table 2. Calculated Parameters for MFC/BT- and CNC/BT-WDFs at Different CNP Concentrations using Bingham Plastic (BP), Power-Law (PL), and Herschel–Bulkley (HB) Models

models			MFC concentration (wt %)				CNCs concentration (wt %)			
		0	0.1	0.25	0.5	1.0	0.1	0.25	0.5	1.0
BP	τ_o	2.74×10^{-5}	5.14×10^{-4}	5.73×10^{-4}	0.85	3.88	0.03	0.87	2.83	6.54
	μ_p	4.82×10^{-3}	5.14×10^{-3}	5.90×10^{-3}	7.50×10^{-3}	0.02	6.80×10^{-3}	8.93×10^{-3}	0.01	0.02
	R^2	0.9646	0.9617	0.9634	0.9715	0.8201	0.98	0.97	0.92	0.84
PL	K	1.95×10^{-4}	1.84×10^{-4}	4.14×10^{-4}	0.16	1.75	2.56×10^{-3}	0.17	1.37	4.10
	n	1.48	1.49	1.39	0.56	0.36	1.14	0.58	0.33	0.24
	R^2	0.9991	0.9988	0.9906	0.9387	0.9808	0.9874	0.9658	0.9582	0.9759
HB	τ_o	0.02	0.02	0.16	0.69	0.88	0.14	0.60	1.77	3.12
	K	1.80×10^{-4}	1.83×10^{-4}	1.85×10^{-4}	0.03	1.22	1.45×10^{-3}	0.05	0.31	1.57
	n	1.49	1.50	1.51	0.81	0.40	1.23	0.75	0.53	0.36
	R^2	0.9992	0.9988	0.997	0.9788	0.9834	0.9905	0.9852	0.9938	0.9920

and CNCs into BT-WDFs dramatically increased the viscosity values from 0.00248 to 0.3796 and 0.738 Pa·s, respectively. The improved viscosity allowed the developed drilling fluids to carry more cuttings, and therefore improved the cutting transport performance of drilling fluids.

MFC/BT- and CNC/BT-WDFs displayed distinctive shear-thinning behaviors, as observed in Figure 1a,b. The shear-thinning behavior for CNC/BT-WDFs was progressive, whereas the shear-thinning behavior for CNC/BT-WDFs was nonprogressive, in which three characteristic regions were observed, corresponding to the orientation of microfibrils along the flow direction at low shear rates, the occurrence of entangled network among microfibrils at moderate shear rates, and the breakage of entangled network at high shear rates, respectively. In comparison with MFC/BT-WDFs, CNC/BT-WDFs exhibited higher viscosity at the same CNP concentrations. For example, at a shear rate of 1 s^{-1}, MFC/BT-WDFs with 0.1, 0.25, 0.5, and 1.0 wt % of MFC had viscosity values of 0.00782, 0.1305, 0.9554, and 1.448 Pa·s, respectively; whereas CNC/BT-WDFs with 0.1, 0.25, 0.5, and 1.0 wt % of CNCs had viscosity values of 0.0423, 0.5479, 2.079, and 4.849 Pa·s, respectively. As observed previously, at the same concentration, MFC suspensions had a substantially higher viscosity than that of CNC suspensions (Figure 1e). Interestingly, when they were mixed with BT suspensions, an opposite trend was observed. Therefore, there must be particular surface interactions existing between CNCs and BT layers, which dramatically improved the resistance of flow upon the shear force.

Figure 2c,d shows the plots of shear stress versus shear rate for MFC/BT- and CNC/BT-WDFs at different CNP concentrations, respectively. Very similar to the viscosity results, the shear stress also enhanced with the increase in the concentration of CNPs, and CNC/BT-WDFs had substantially higher shear stress than MFC/BT-WDFs at the same concentration. The Bingham plastic, power-law and Herschel–Bulkey models were applied to fit their shear stress–shear rate curves, and the corresponding fit parameters are summarized in Table 2. In comparison with the Bingham plastic and power-law models, the Herschel–Bulkey model provided a better fit for the shear stress–shear rate curves, which was evidenced by the higher values of R^2 (closer to 1).[7] It can be seen that MFC/BT-WDFs with 0.1, 0.25, 0.5, and 1.0 wt % of MFC had yield point values of 0.02, 0.16, 0.69, and 0.88 Pa, respectively; whereas CNC/BT-WDFs with 0.1, 0.25, 0.5, and 1.0 wt % of CNCs had yield point values of 0.14, 0.60, 1.77, and 3.12 Pa, respectively. CNC/BT-WDFs had higher yield point values than MFC/BT-WDFs. The yield point, the stress required to start the flow of drilling fluid, is also used by drilling engineers to predict the capacity of drilling fluid to transport the cuttings to surface. Therefore, rheological modeling results also demonstrated that the incorporation of CNP improved the wellbore cleaning efficiency of BT-WDFs, and CNC/BT-WDFs had superior cutting transport performance to MFC/BT-WDFs.

Based on the above observations, it can be concluded that CNC/BT-WDFs exhibited better rheological properties than MFC/BT-WDFs, presumably due to the formation of particular surface interactions between CNCs and BT layers. Now, the questions were arisen as to what the driving force is inducing such strong surface interactions between CNCs and BT layers in aqueous solution, or if this driving force existed in both MFC/BT and CNC/BT systems, why the surface interactions between CNCs and BT layers were stronger than those between MFC and BT. With these questions, the microstructures of MFC/BT- and CNC/BT-WDFs were examined by TEM observations, as displayed in Figure 3. Interestingly, distinctive dispersion states and phase interactions were observed between MFC/BT- and CNC/BT-WDFs. In the MFC/BT-WDFs, BT was exfoliated into single layers and

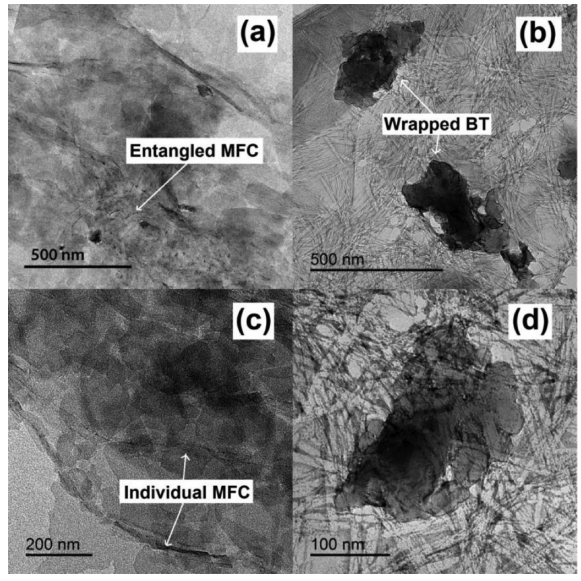

Figure 3. TEM micrographs of (a and b) MFC/BT-, and (c and d) CNC/BT-WDFs. (The concentration of CNP in BT-WDFs was 0.5 wt %, and then the fluids were diluted 10 times using deionized water.)

DOI: 10.1021/acsami.5b00498
ACS Appl. Mater. Interfaces 2015, 7, 5006–5016

homogeneously dispersed as the matrix. Similar to the MFC suspension (Figure 1a), two main dispersion states of microfibrils were observed, i.e., most of microfibrils were still highly entangled to form strong network (Figure 3a) and only a few individual microfibrils well dispersed within the exfoliated BT layers (Figure 3c). By contrast, in the CNC/BT-WDFs, BT aggregations with particle size approximate 250−500 nm were significantly wrapped by layers of CNCs, forming a particular "core−shell" structure (Figure 3b,d). Based on these observations, a core−shell model was proposed for CNC/BT-WDFs, as shown in Figure 4.

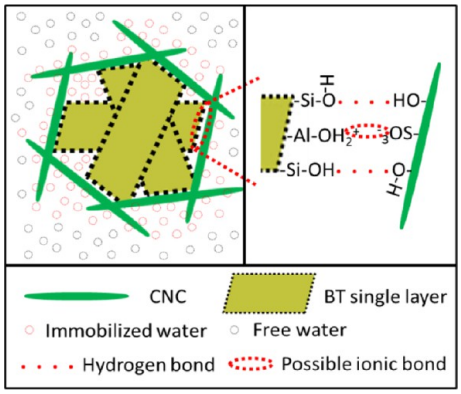

Figure 4. Proposed core−shell model for CNC/BT-WDFs.

It has been reported that BT was composed of a large number of plate-like layers with a permanent negative charge on the flat surface and pH-dependent charge on the edge.[12,45] Due to the broken bonds of the octahedral Al layers and tetrahedral Si layers on the edge, the amphoteric Al−OH and Si−OH groups were present, which were conditionally charged to be negative, neutral or positive. Generally, at a high pH value, the edge (Al−O^-) was negatively charged; at a moderate pH value, the edge (Al−OH) was neutral; at a low pH value, the edge (Al−OH_2^+) was positively charged. However, in a neutral condition, a positive charged edge could be also possibly created due to the exposed octahedral Al layers.[45,46] The ionic attraction between the negatively charged flat surface and positively charged edge (edge-to-face attractions) formed a "house of card" structure, which was responsible for the viscosity of BT suspensions.[47] CNCs exhibited strongly hydrophilic and negatively charged surface properties due to the presence of hydroxyl and sulfate groups (Table 1). It can be expected that when CNCs and BT were mixed in aqueous solution, CNCs could immediately attach to the edge of BT layers via the formation of hydrogen bond between their hydroxyl groups, and the possible ionic bond between the positively charged edge site of BT layers and the negatively charged sulfate groups of CNCs,[48] as illustrated in Figure 4. As more and more CNCs were attached to the edge of BT, BT layers were significantly wrapped by CNCs, resulting in the observed core−shell structure. On the other hand, because of the high surface area and a large number of hydroxyl groups on the surface, CNCs had a strong gel formation capacity. A large number of water molecules were bounded at the vicinity of CNCs via hydrogen bond.[49,50] Therefore, a stiff network among BT layers, CNCs, and immobilized water molecules was created, which had a strong resistance to flow under shear force, leading to a significant improvement in the rheological properties. By contrast, because the present MFC was prepared through the mechanical disintegration process, their surface was quite intact with fewer hydroxyl groups and lack of negatively charged sulfate group. It can be expected that the surface interactions mainly resulting from hydrogen bond between MFC and BT layers were weaker than those between CNCs and BT layers. Moreover, the highly entangled structure strongly prohibited the mobility of microfibrils. Therefore, in MFC/BT-WDFs, it is very difficult to form the core−shell structure due to the weak surface interaction and poor mobility.

If the core−shell structure indeed existed in CNC/BT-WDFs, they could show a particular pH-responsive behavior.[51] It is expected that at a low pH, more positively charged sites were created on the edge of BT layers,[12,45] leading to stronger ionic interaction between CNCs and BT layers. By contrast, because MFC had a very low negative charge (Table 1), it is expected that the change in the pH had little influence on the surface interaction between MFC and BT. The influence of pH on the viscosity of MFC/BT- and CNC/BT-WDFs was investigated, as shown in Figures 5a,b, respectively. At the low shear rate, both MFC/BT- and CNC/BT-WDFs showed high stability in the viscosity upon the change in the pH values from 11.0 to 4.4. It is postulated that when the shear rate was low, the contribution of surface interactions on the viscosity was slight. As the shear rate increased, the viscosity significantly decreased. At this time, the surface interactions between CNP and BT acted as crucial role in the maintenance of viscosity. As a result, at the high shear rate, CNC/BT-WDFs exhibited more sensitivity to the pH change than MFC/BT-WDFs. As shown in Figure 5a and 5b, when the pH was decreased to 4.4, at the

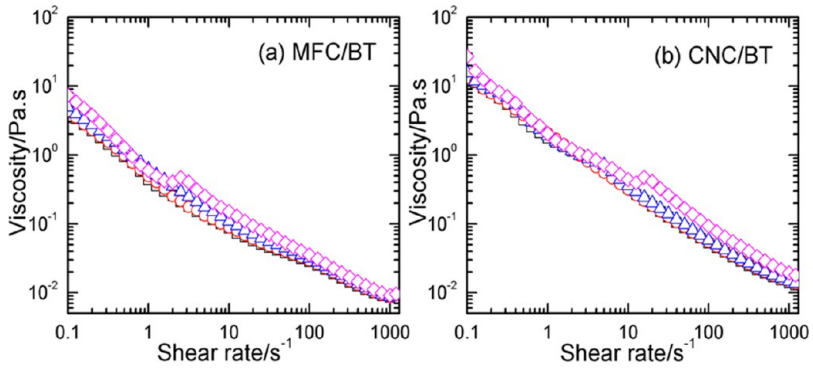

Figure 5. Effect of pH on the viscosity of (a) MFC/BT- and (b) CNC/BT-WDFs at pH of 11.0 (black squares), 8.9 (red circles), 6.7 (blue triangles), and 4.4 (magenta diamonds) with a fixed CNP concentration of 0.5 wt %.

DOI: 10.1021/acsami.5b00498
ACS Appl. Mater. Interfaces 2015, 7, 5006−5016

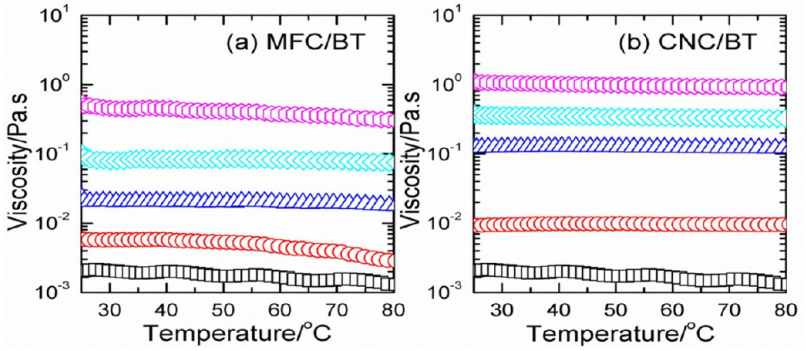

Figure 6. Effect of temperature on the viscosity of (a) MFC/BT-, and (b) CNC/BT-WDFs at different CNP concentrations: 0 wt % (black squares), 0.1 wt % (red circles), 0.25 wt % (blue triangles), 0.5 wt % (cyan diamonds) and 1.0 wt % (magenta hexagons) at a fixed shear rate of 10 s^{-1}.

shear rate ranging from 100 to 1200 s^{-1}, the change in the viscosity of MFC/BT-WDFs was not profound; whereas an evident increase in the viscosity was observed for CNC/BT-WDFs due to the formation of denser core−shell structure resulting from stronger ionic attraction between CNCs and BT interfaces.

The strong surface interaction of CNC/BT-WDFs can be further evidenced by the investigation on the dependence of viscosity upon the change in the temperature. Generally, when the temperature was elevated, the viscosity of WDFs declined due to the increase in the mobility of water molecules. However, if there were some strong surface interactions occurring in the WDFs, they could be less sensitive to the change in the temperature.[8] Figure 6a,b shows the effect of temperature on the viscosity of MFC/BT- and CNC/BT-WDFs, respectively. It can be seen that without the addition of CNPs, the viscosity of BT-WDFs was quite unstable with change in the temperature. MFC/BT-WDFs also exhibited poor thermal stability, especially at a low concentration, such as 0.1 wt %, in which the viscosity significantly declined starting from 60 °C. However, for CNC/BT-WDFs at any concentration of CNC, their viscosity were well maintained over a broad range of temperature from 20 to 80 °C, owing to the formation of stiff network among BT layers, CNCs, and immobilized water molecules, in which water molecules could be entrapped within the core−shell structure and immobilized at the vicinity of CNCs, leading to more resistance to the temperature change.[8] As the wellbore being drilled deeper, much heat was released due to the excessive friction between the drilling bit and the formation, leading to significant increase in the temperature of wellbore. In order to maintain the cutting transport performance of drilling fluids, it is very essential to develop the drilling fluids with the minimum temperature effect. Therefore, in comparison to MFC, CNCs were also advantageous for the high temperature drilling fluid application.

It is well-known that the penetration of fluids into the formation could result in significant swelling and subsequently cause serious wellbore collapse.[5,52] Furthermore, the flocculation (filter cake) deposited on the wall of wellbores leads to high probability of differential pressure sticking, well damage, and stuck pipe problems.[11,52] Therefore, a suitable drilling fluid should also have desirable filtration properties, e.g., low filtrate volume as well as thin and dense filter cake. Figure 7a,b shows the fluid loss volume as a function of time for MFC/BT- and CNC/BT-WDFs at different CNP concentrations, respectively. The original BT-WDFs had a high fluid loss volume of 34.6 mL. Obviously, the incorporation of MFC and CNCs into BT-

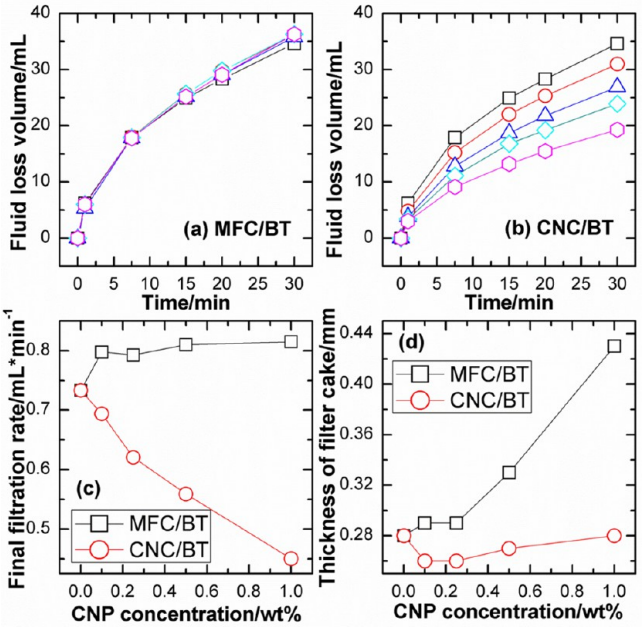

Figure 7. Plots of (a and b) fluid loss volume versus time for MFC/BT- and CNC/BT-WDFs at different CNP concentrations: 0 wt % (black squares), 0.1 wt % (red circles), 0.25 wt % (blue triangles), 0.5 wt % (cyan diamonds) and 1.0 wt % (magenta hexagons), respectively. (c and d) Final filtration rate and thickness of dried filter cake versus CNP concentration, respectively.

WDFs also led to distinctive fluid loss properties. MFC had little impact on the fluid loss volume; whereas the fluid loss volume gradually decreased as the concentration of CNCs increased from 0.1 to 1.0 wt %. For example, CNC/BT-WDFs with 0.1, 0.25, 0.5, and 1.0 wt % of CNCs had fluid loss volume of 31.0, 26.9, 23.9, and 19.3 mL, showing a decrease of 10.4, 22.3, 30.9, and 44.2%, respectively, when compared to the original BT-WDFs. Moreover, it was observed that the plot of fluid loss volume versus time from 7.5 to 30 min was nearly linear. Thus, the slope of each plot from 7.5 to 30 min was calculated and defined as its final filtration rate, as depicted in Figure 7c. It can be seen that the final filtration rate increased from 0.73 to 0.80 mL/min with the incorporation of 0.1 wt % of MFC, after which the final filtration rate appeared to level off. In a sharp contrast, the final filtration rate continuously decreased from 0.73 to 0.69, 0.62, 0.56, and 0.45 mL/min in the presence of CNCs with concentration of 0.1, 0.25, 0.5, and 1.0 wt %, respectively. These results demonstrated MFC gave a

DOI: 10.1021/acsami.5b00498
ACS Appl. Mater. Interfaces 2015, 7, 5006−5016

slight detrimental effect in the fluid loss reduction, while CNCs yielded a significant improvement in the fluid loss reduction.

The thickness of filter cakes after 24 h evaporation was also measured, as plotted in Figure 7d. The original BT-WDF deposited a filter cake with a thickness of 0.28 mm. MFC/BT-WDFs experienced a slight increase in the thickness of filter cakes from 0.1 to 0.25 wt %, after which they exhibited a steep increase in the thickness from 0.5 to 1.0 wt %. CNC/BT-WDFs showed a slight decrease in the thickness of filter cakes from 0.1 to 0.25 wt %, after which their thickness slightly increased from 0.5 to 1.0 wt %. At the same concentration, CNC/BT-WDFs yielded much thinner filter cake than MFC/BT-WDFs, especially at a high concentration. Figure 8 shows the photographs of fresh filter cakes. The color of filter cake was gradually changed from dark to white due to more and more CNP deposited on the filter paper with the increase in the CNP concentrations. MFC/BT-WDFs formed loose and open filter cakes, as evidenced by the observation that the sediments tended to flow out of the filter cakes to the margin of filter papers. By contrast, CNC/BT-WDFs created relatively dense and compact filter cakes, since there were no sediments observed at the margin of filter papers.

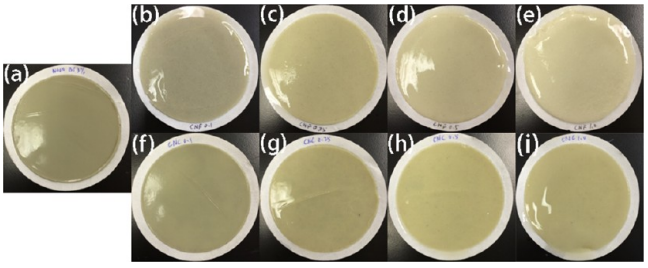

Figure 8. Digital images of fresh filter cakes: (a) BT; (b), (c), (d), and (e) MFC/BT with MFC concentration of 0.1, 0.25, 0.5, and 1.0 wt %, respectively; (f), (g), (h), and (i) CNC/BT with MFC concentration of 0.1, 0.25, 0.5, and 1.0 wt %, respectively. (Images were taken immediately after each API fluid loss testing.)

Filtration measurements demonstrated that MFC resulted in little impact on the fluid loss volume as well as thick, loose, and open filter cakes; whereas CNCs yielded a profound reduction in the fluid loss volume as well as thin, dense and compact filter cakes. The reasons for such distinctive phenomena were proposed in detail as follows. First, CNC/BT-WDFs had a higher viscosity than MFC/BT-WDFs (Figure 2). The improved viscosity slowed down the rate of filtration and flocculation.[53,54] Second, the created core−shell structure in CNC/BT-WDFs (Figure 3) not only encapsulated and bound enormous amounts of water molecules but also wrapped BT against flocculation.[8] Third, the addition of CNCs and MFC might modify the microstructure of filter cakes, leading to the change in the permeability.[20] To see whether the presence of CNCs and MFC had impact on the microstructure of filter cakes, the dried filter cakes were analyzed using FE-SEM, as shown in Figure 9. Clearly, no CNPs were observed on the surface of filter cake flocculated from BT-WDFs (Figure 9a,b). For the filter cakes flocculated from MFC/BT- and CNC/BT-WDFs, distinctive morphologies were observed. MFC agglomerated into microsize bundles and randomly dispersed in the BT matrix (Figure 9c,d), while CNCs formed thin polymer films covering the surface of the BT matrix (Figure 9e,f). It is postulated that this typically generated CNC polymer films contributed to the closing of fluid penetration channels, leading to the significant improvement in the filtration properties, too.

In summary, the addition of CNPs improved the rheological and filtration properties of BT-WDFs, and CNC/BT-WDFs exhibited superior performances compared to MFC/BT-WDFs. Finally, in order to show how effective the CNC/BT-WDFs were, the performances of CNC/BT-WDFs with 0.5 wt % of CNCs and 3 wt % of BT were compared with those of BT-WDFs with higher BT concentrations ranging from 3 to 15 wt %, as presented in Table 3. With an increase in the

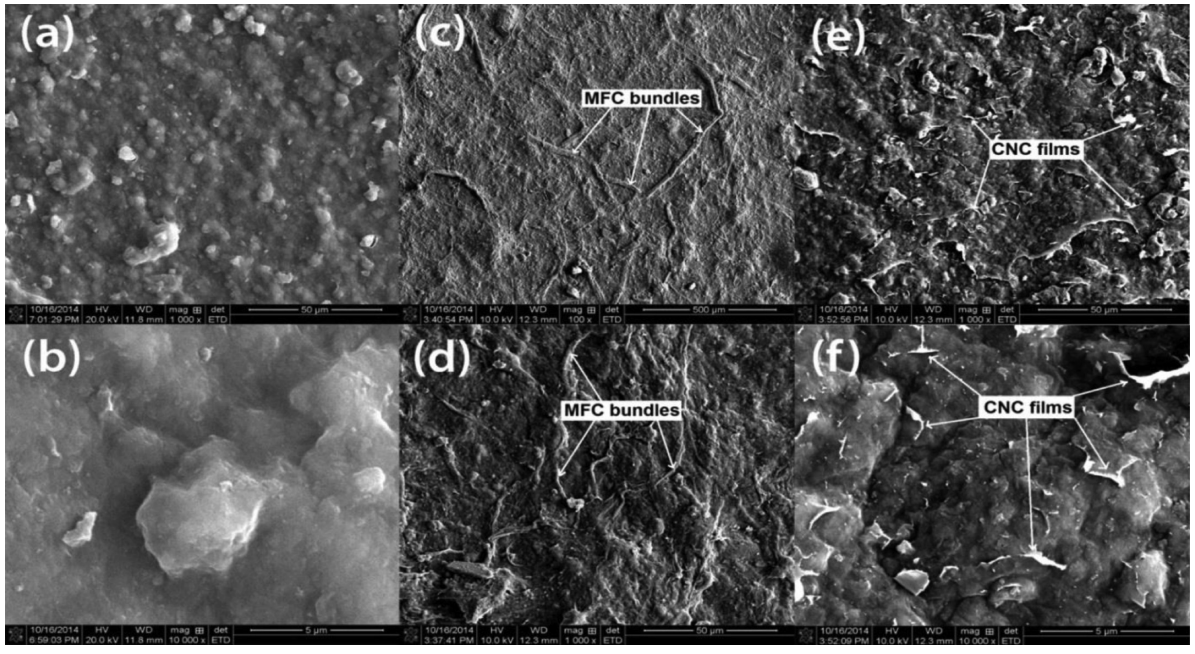

Figure 9. FE-SEM micrographs of dried filter cakes deposited on the filter papers from (a and b) BT, (c and d) MFC/BT-, and (e and f) CNC/BT-WDFs. Scale bar: (a, d, and e) 50 μm; (b and f) 5 μm; (c) 100 μm. CNP concentration: 1.0 wt %.

DOI: 10.1021/acsami.5b00498
ACS Appl. Mater. Interfaces 2015, 7, 5006−5016

Table 3. Rheological[a] and Filtration Properties of BT-, CNC/BT-, and CNC/PAC/BT-WDFs

drilling fluids	AP (cP)	PV (cP)	YP (N/m^2)	Gel_{in} (N/m^2)	Gel_{10min} (N/m^2)	FL[b] (mL)	TC[c] (mm)
BT 3%	2.1	1.5	1.0	1.0	1.2	34.6	0.28
BT 6%	5.5	5.2	1.1	1.2	2.1	22.9	0.32
BT 7.5%	7.1	5.8	2.3	1.5	4.3	19.5	0.35
BT 12%	42.3	30.7	21.8	9.6	28.4	13.7	0.71
BT 15%	137.4	83.2	77.6	64.8	96.3	12.0	1.03
BT 3% + CNC 0.5%	7.6	4.4	7.6	1.8	4.8	23.9	0.27
BT3%+CNC0.5%+PAC0.1%	8.9	5.6	10.2	2.1	6.3	16.8	0.20
BT3%+CNC 0.5%+PAC0.5%	31.4	19.8	20.4	7.2	20.1	13.0	0.15
BT 3% + CNC 1.0%	17.5	10.3	14.7	4.8	15.2	19.8	0.28

[a]Measured using the NL Baroid viscometer. [b]FL: fluid loss. [c]TC: thickness of filter cake.

concentration of BT from 3 to 15 wt %, the AP, PV, YP, Gel_{in}, $Gel_{10\ min}$, and thickness of filter cake gradually increased, while the fluid loss continuously decreased. High concentration of BT led to thicker of filter cakes, which can cause serious differential pressure sticking, well damage, and stuck pipe problems. This is why high concentration of BT should be avoided. It can be seen that CNC/BT-WDFs displayed the similar rheological properties as 7.5 wt % BT-WDFs, the similar fluid loss volume as 6 wt % BT-WDFs, and the similar thickness of filter cake as 3 wt % BT-WDFs. Thus, the required rheological and filtration properties can be achieved with less amount of BT by addition of a small amount of CNCs. PAC is a common fluid loss reducer used in WDFs. PAC was added into CNC/BT-WDFs to see whether they can further decrease the fluid loss volume and the thickness of filter cakes. Gratifyingly, the incorporation of 0.1 and 0.5 wt % of PAC into CNC/BT-WDFs remarkably decreased the fluid loss volume and thickness of filter cake to 16.8 mL/0.20 mm and 13.0 mL/0.15 mm, respectively. Furthermore, the PAC/CNC/BT-WDFs exhibited superior rheological properties than CNC/BT-WDFs, showing a synergistic effect of CNCs and PAC on the performance improvement of BT-WDFs.

CONCLUSIONS

CNCs were extracted from MFC using the 64 wt % sulfur acid hydrolysis. The resultant CNCs exhibited distinctive characteristics with MFC such as smaller dimensions, more negative charges on the surface, higher stability in aqueous solution, but lower viscosity, and less evident shear thinning behaviors. Both MFC and CNCs were utilized as clean, cheap, renewable, recyclable, biodegradable, and environmentally friendly additives to improve the rheological and filtration properties of BT-WDFs. The addition of MFC and CNCs increased the rheological properties of BT-WDFs, including the viscosity, shear stress, and yield point, demonstrating the development in the cuttings transport capacity. A typical core−shell structure was observed in CNC/BT-WDFs due to the strong surface interaction among BT layers, CNCs, and immobilized water molecules. A similar structure was not seen in MFC/BT-WDFs. At a low pH, more positively charged sites were formed on the edge of BT, leading to stronger ionic bond, denser core−shell structure, and stiffer network in CNC/BT-WDFs. The created core−shell structure enabled CNC/BT-WDFs to have more resistance to the temperature change, indicating their potential for high temperature WDFs application. Moreover, the improved viscosity, the created core−shell structure as well as the formation of CNC polymer films remarkably reduced the fluid loss volume and the thickness of filter cake for CNC/BT-WDFs. By contrast, MFC had little impact on the fluid loss volume, and yielded thicker filter cakes, which can cause serious problems such as differential pressure sticking, well damage, and stuck pipe. To summarize, CNCs yielded better rheological and filtration performances than MFC in BT-WDFs application.

The performances of CNC/BT-WDFs were compared with those of BT-WDFs with higher concentrations of BT. It was observed that with the addition of a small amount of CNCs, more BT can be saved in order to achieve the required rheological and filtration properties. Furthermore, a synergistic effect of PAC and CNCs on the performance improvement in the BT-WDFs was observed. This research compares the rheological and filtration properties of MFC/BT- and CNC/BT-WDFs, and demonstrates the effectiveness of CNCs in enhancing the performances of BT-WDFs, opening a pathway of a new generation of additives in well-drilling fluid applications.

AUTHOR INFORMATION

Corresponding Authors

*Q. Wu. E-mail: qwu@agcenter.lsu.edu. Phone: 225-578-8369. Fax: 225-578-4251.

*Y. Wu. E-mail: wuyiqiang@csuft.edu.cn. Phone: 731-85623301. Fax: 731-85623301.

Author Contributions

The paper was written through contributions of all authors. All authors have given approval to the final version of the paper.

Notes

The authors declare no competing financial interest.

ACKNOWLEDGMENTS

This collaborative study was carried out with support from the Louisiana Board of Regents [LEQSF-EPS (2014)-OPT-IN-37, LEQSF (2010-15)-RD-B-01; LEQSF(2013-14)-ENH-TR-02], Louisiana State University EDA program, and Central South University of Forestry and Technology, Changsha, China.

REFERENCES

(1) Bailey, L.; Keall, M.; Audibert, A.; Lecourtier, J. Effect of Clay/Polymer Interactions on Shale Stabilization during Drilling. *Langmuir* **1994**, *10*, 1544−1549.

(2) Jones, T. G. J.; Hughes, T. L. Drilling Fluid Suspensions. In *Suspensions: Fundamentals and Applications in the Petroleum Industry*; Advances in Chemistry Series; American Chemical Society: Washington, DC, 1996; Vol. *251*, pp 10−463.

(3) Baba Hamed, S.; Belhadri, M. Rheological Properties of Biopolymers Drilling Fluids. *J. Pet. Sci. Eng.* **2009**, *67*, 84−90.

(4) Kelessidis, V. C.; Poulakakis, E.; Chatzistamou, V. Use of Carbopol 980 and Carboxymethyl Cellulose Polymers as Rheology

DOI: 10.1021/acsami.5b00498
ACS Appl. Mater. Interfaces 2015, 7, 5006−5016

Modifiers of Sodium-Bentonite Water Dispersions. *Appl. Clay Sci.* **2011**, *54*, 63−69.
(5) Kosynkin, D. V.; Ceriotti, G.; Wilson, K. C.; Lomeda, J. R.; Scorsone, J. T.; Patel, A. D.; Friedheim, J. E.; Tour, J. M. Graphene Oxide as a High-Performance Fluid-Loss-Control Additive in Water-based Drilling Fluids. *ACS Appl. Mater. Interfaces* **2011**, *4*, 222−227.
(6) Wan, T.; Yao, J.; Zishun, S.; Li, W.; Juan, W. Solution and Drilling Fluid Properties of Water Soluble AM−AA−SSS Copolymers by Inverse Microemulsion. *J. Pet. Sci. Eng.* **2011**, *78*, 334−337.
(7) Khalil, M.; Mohamed Jan, B. Viscoplastic Modeling of a Novel Lightweight Biopolymer Drilling Fluid for Underbalanced Drilling. *Ind. Eng. Chem. Res.* **2012**, *51*, 4056−4068.
(8) Yan, L.; Wang, C.; Xu, B.; Sun, J.; Yue, W.; Yang, Z. Preparation of a Novel Amphiphilic Comb-like Terpolymer as Viscosifying Additive in Low-Solid Drilling Fluid. *Mater. Lett.* **2013**, *105*, 232−235.
(9) Okon, A. N.; Udoh, F. D.; Bassey, P. G. Evaluation of Rice Husk as Fluid Loss Control Additive in Water-based Drilling Mud. *Nigeria Annual International Conference and Exhibition*, Lagos, Nigeria, August 5−7, 2014; Society of Petroleum Engineers: London, 2014; SPE Paper No. 172379.
(10) Kelessidis, V. C.; Zografou, M.; Chatzistamou, V. Optimization of Drilling Fluid Rheological and Fluid Loss Properties Utilizing PHPA Polymer. *Middle East Oil and Gas Show and Conference*, Manama, Bahrain, March 8−11, 2013; Society of Petroleum Engineers: Dubai, 2013; SPE Paper No. 164351.
(11) Zakaria, M.; Husein, M. M.; Harland, G. Novel Nanoparticle-based Drilling Fluid with Improved Characteristics. *International Oilfield Nanotechnology Conference and Exhibition*, Noordwijk, The Netherlands, June 12−14, 2012; Society of Petroleum Engineers: London, 2012; SPE Paper No. 156992.
(12) Jung, Y.; Son, Y.-H.; Lee, J.-K.; Phuoc, T. X.; Soong, Y.; Chyu, M. K. Rheological Behavior of Clay−Nanoparticle Hybrid-Added Bentonite Suspensions: Specific Role of Hybrid Additives on the Gelation of Clay-based Fluids. *ACS Appl. Mater. Interfaces* **2011**, *3*, 3515−3522.
(13) Fan, J.; Zhu, H.; Li, R.; Chen, N. Montmorillonite Modified by Cationic and Nonionic Surfactants as High-Performance Fluid-Loss-Control Additive in Oil-based Drilling Fluids. *J. Dispers. Sci. Technol.* **2014**, *36*, 569−576.
(14) William, J. K. M.; Ponmani, S.; Samuel, R.; Nagarajan, R.; Sangwai, J. S. Effect of CuO and ZnO Nano Fluids in Xanthan Gum on Thermal, Electrical and High Pressure Rheology of Water-based Drilling Fluids. *J. Pet. Sci. Eng.* **2014**, *117*, 15−27.
(15) Dias, F. T. G.; Souza, R. R.; Lucas, E. F. Influence of Modified Starches Composition on Their Performance as Fluid Loss Additives in Invert-Emulsion Drilling Fluids. *Fuel* **2015**, *140*, 711−716.
(16) Anderson, R. W.; Barker, J. R. Use of Guar Gum and Synthetic Cellulose in Oilfield Stimulation Fluids. *Fall Meeting of the Society of Petroleum Engineers of AIME*, Houston, TX, October 6−9, 1974; Society of Petroleum Engineers: Richardson, TX, 1974; SPE Paper No. 5005.
(17) Navarrete, R. C.; Himes, R. E.; Seheult, J. M. Applications of Xanthan Gum in Fluid-Loss Control and Related Formation Damage. *SPE Permian Basin Oil and Gas Recovery Conference*, Midland, TX, March 23−26, 2000; Society of Petroleum Engineers: Richardson, TX, 2000; SPE Paper No. 59535.
(18) Menezes, R. R.; Marques, L. N.; Campos, L. A.; Ferreira, H. S.; Santana, L. N. L.; Neves, G. A. Use of Statistical Design to Study the Influence of CMC on the Rheological Properties of Bentonite Dispersions for Water-based Drilling Fluids. *Appl. Clay Sci.* **2010**, *49*, 13−20.
(19) Mahto, V.; Sharma, V. P. Rheological Study of a Water based Oil Well Drilling Fluid. *J. Pet. Sci. Eng.* **2004**, *45*, 123−128.
(20) Warren, B.; van der Horst, P.; Stewart, W. Application of Amphoteric Cellulose Ethers in Drilling Fluids. *International Symposium on Oilfield Chemistry*, Houston, TX, February 20−21, 2003; Society of Petroleum Engineers: Richardson, TX, 2003; SPE Paper No. 80210.
(21) Nunes, R. de C. P.; Pires, R. V.; Lucas, E. F.; Vianna, A.; Lomba, R. New Filtrate Loss Controller Based on Poly(methyl methacrylate-co-vinyl acetate). *J. Appl. Polym. Sci.* **2014**, *131*.
(22) Fazelabdolabadi, B.; Khodadadi, A.; Sedaghatzadeh, M. Thermal and Rheological Properties Improvement of Drilling Fluids Using Functionalized Carbon Nanotubes. *Appl. Nanosci.* **2014**, 1−9.
(23) Cai, J.; Chenevert, M. E.; Sharma, M. M.; Friedheim, J. E. Decreasing Water Invasion Into Atoka Shale Using Nonmodified Silica Nanoparticles. *SPE Drill. Completion* **2012**, *27*, 103−112.
(24) Pääkkö, M.; Ankerfors, M.; Kosonen, H.; Nykänen, A.; Ahola, S.; Österberg, M.; Ruokolainen, J.; Laine, J.; Larsson, P. T.; Ikkala, O.; Lindstrom, T. Enzymatic Hydrolysis Combined with Mechanical Shearing and High-Pressure Homogenization for Nanoscale Cellulose Fibrils and Strong Gels. *Biomacromolecules* **2007**, *8*, 1934−1941.
(25) Saito, T.; Nishiyama, Y.; Putaux, J.-L.; Vignon, M.; Isogai, A. Homogeneous Suspensions of Individualized Microfibrils from TEMPO-Catalyzed Oxidation of Native Cellulose. *Biomacromolecules* **2006**, *7*, 1687−1691.
(26) Yao, X.; Qi, X.; He, Y.; Tan, D.; Chen, F.; Fu, Q. Simultaneous Reinforcing and Toughening of Polyurethane via Grafting on the Surface of Microfibrillated Cellulose. *ACS Appl. Mater. Interfaces* **2014**, *6*, 2497−2507.
(27) Xu, X.; Liu, F.; Jiang, L.; Zhu, J. Y.; Haagenson, D.; Wiesenborn, D. P. Cellulose Nanocrystals vs. Cellulose Nanofibrils: A Comparative Study on Their Microstructures and Effects as Polymer Reinforcing Agents. *ACS Appl. Mater. Interfaces* **2013**, *5*, 2999−3009.
(28) Han, J.; Zhou, C.; Wu, Y.; Liu, F.; Wu, Q. Self-Assembling Behavior of Cellulose Nanoparticles during Freeze-Drying: Effect of Suspension Concentration, Particle Size, Crystal Structure, and Surface Charge. *Biomacromolecules* **2013**, *14*, 1529−1540.
(29) Zhou, C.; Shi, Q.; Guo, W.; Terrell, L.; Qureshi, A. T.; Hayes, D. J.; Wu, Q. Electrospun Bio-Nanocomposite Scaffolds for Bone Tissue Engineering by Cellulose Nanocrystals Reinforcing Maleic Anhydride Grafted PLA. *ACS Appl. Mater. Interfaces* **2013**, *5*, 3847−3854.
(30) Liu, A.; Walther, A.; Ikkala, O.; Belova, L.; Berglund, L. A. Clay Nanopaper with Tough Cellulose Nanofiber Matrix for Fire Retardancy and Gas Barrier Functions. *Biomacromolecules* **2011**, *12*, 633−641.
(31) Benítez, A. J.; Torres-Rendon, J.; Poutanen, M.; Walther, A. Humidity and Multiscale Structure Govern Mechanical Properties and Deformation Modes in Films of Native Cellulose Nanofibrils. *Biomacromolecules* **2013**, *14*, 4497−4506.
(32) Martínez-Sanz, M.; Lopez-Rubio, A.; Lagaron, J. M. Optimization of the Dispersion of Unmodified Bacterial Cellulose Nanowhiskers into Polylactide via Melt Compounding to Significantly Enhance Barrier and Mechanical Properties. *Biomacromolecules* **2012**, *13*, 3887−3899.
(33) Liu, H.; Liu, D.; Yao, F.; Wu, Q. Fabrication and Properties of Transparent Polymethylmethacrylate/Cellulose Nanocrystals Composites. *Bioresour. Technol.* **2010**, *101*, 5685−5692.
(34) Hamad, W. Y.; Hu, T. Q. Structure−Process−Yield Interrelations in Nanocrystalline Cellulose Extraction. *Can. J. Chem. Eng.* **2010**, *88*, 392−402.
(35) Nasiri, M.; Ashrafizadeh, S. N. Novel Equation for the Prediction of Rheological Parameters of Drilling Fluids in an Annulus. *Ind. Eng. Chem. Res.* **2010**, *49*, 3374−3385.
(36) American Petroleum Institute. *Recommended Practice for Field Testing of Water-Based Drilling Fluids*, 3rd ed.; American Petroleum Institute: Washington, DC, 2003 (November 1, 2003, 82 pages, ANSI/API 13B-1).
(37) Lin, N.; Dufresne, A. Surface Chemistry, Morphological Analysis and Properties of Cellulose Nanocrystals with Gradiented Sulfation Degrees. *Nanoscale* **2014**, *6*, 5384−5393.
(38) Dickinson, E. In *Basic Principles of Colloid Science*; Everett, D. H., Ed.; Royal Society of Chemistry: London, 1988.
(39) Plank, J.; Keilhofer, G.; Lange, P. MMH-Bentonite Fluids Provide Outstanding Performance in Oil Field Drilling. *Oil Gas J.* **2000**, *98*, 39−42.

DOI: 10.1021/acsami.5b00498
ACS Appl. Mater. Interfaces 2015, 7, 5006−5016

(40) Lyons, W. *Working Guide to Drilling Equipment and Operations*; Gulf Professional Publishing: Houston, TX, 2009.
(41) Bischoff White, E.; Chellamuthu, M.; Rothstein, J. Extensional Rheology of a Shear-Thickening Cornstarch and Water Suspension. *Rheol. Acta* **2010**, *49*, 119−129.
(42) Laun, H. M. Rheological Properties of Aqueous Polymer Dispersions. *Die Angew. Makromol. Chem.* **1984**, *123*, 335−359.
(43) Khandavalli, S.; Rothstein, J. P. Extensional Rheology of Shear-Thickening Fumed Silica Nanoparticles Dispersed in an Aqueous Polyethylene Oxide Solution. *J. Rheol.* **2014**, *58*, 411−431.
(44) Hoffman, R. L. Discontinuous and Dilatant Viscosity Behavior in Concentrated Suspensions. I. Observation of a Flow Instability. *Trans. Soc. Rheol.* **1972**, *16*, 155−173.
(45) Luckham, P. F.; Rossi, S. The Colloidal and Rheological Properties of Bentonite Suspensions. *Adv. Colloid Interface Sci.* **1999**, *82*, 43−92.
(46) Hunter, R. J.; Alexander, A. E. Surface Properties and Flow Behavior of Kaolinite. Part III: Flow of Kaolinite Sols through a Silica Column. *J. Colloid Sci.* **1963**, *18*, 846−862.
(47) Lagaly, G. Principles of Flow of Kaolin and Bentonite Dispersions. *Appl. Clay Sci.* **1989**, *4*, 105−123.
(48) Wu, C.-N.; Saito, T.; Fujisawa, S.; Fukuzumi, H.; Isogai, A. Ultrastrong and High Gas-Barrier Nanocellulose/Clay-Layered Composites. *Biomacromolecules* **2012**, *13*, 1927−1932.
(49) Ono, H.; Shimaya, Y.; Sato, K.; Hongo, T. ^{1}H Spin-Spin Relaxation Time of Water and Rheological Properties of Cellulose Nanofiber Dispersion, Transparent Cellulose Hydrogel (TCG). *Polym. J.* **2004**, *36*, 684−694.
(50) Benhamou, K.; Dufresne, A.; Magnin, A.; Mortha, G.; Kaddami, H. Control of Size and Viscoelastic Properties of Nanofibrillated Cellulose From Palm Tree by Varying the TEMPO-Mediated Oxidation Time. *Carbohydr. Polym.* **2014**, *99*, 74−83.
(51) Way, A. E.; Hsu, L.; Shanmuganathan, K.; Weder, C.; Rowan, S. J. pH-Responsive Cellulose Nanocrystal Gels and Nanocomposites. *ACS Macro Lett.* **2012**, *1*, 1001−1006.
(52) Blkoor, S. O.; Ka, F. The Influence of XC-Polymer on Drilling Fluid Filter Cake Properties and Formation Damage. *J. Pet. Environ. Biotechnol.* **2013**, *04*.
(53) Desbrieres, J. Cement Cake Properties in Static Filtration. Influence of Polymeric Additives on Cement Filter Cake Permeability. *Cem. Concr. Res.* **1993**, *23*, 347−358.
(54) Desbrieres, J. Cement Cake Properties in Static Filtration. On the Role of Fluid Loss Control Additives on the Cake Porosity. *Cem. Concr. Res.* **1993**, *23*, 1431−1442.

DOI: 10.1021/acsami.5b00498
ACS Appl. Mater. Interfaces 2015, 7, 5006−5016